

See discussions, stats, and author profiles for this publication at: <https://www.researchgate.net/publication/390105132>

Spatiotemporal mass change rate analysis from 2002 to 2023 over the Antarctic Ice Sheet and four glacier basins in Wilkes–Queen Mary Land

Article in *Science China Earth Sciences* · March 2025

DOI: 10.1007/s11430-024-1517-1

CITATIONS

0

READS

545

5 authors, including:



Wei Wang

Tongji University

17 PUBLICATIONS 114 CITATIONS

[SEE PROFILE](#)



Yunzhong Shen

Tongji University

232 PUBLICATIONS 3,597 CITATIONS

[SEE PROFILE](#)



Qiuqie Chen

Tongji University

79 PUBLICATIONS 617 CITATIONS

[SEE PROFILE](#)



Fengwei Wang

Tongji University

68 PUBLICATIONS 353 CITATIONS

[SEE PROFILE](#)

Spatiotemporal mass change rate analysis from 2002 to 2023 over the Antarctic Ice Sheet and four glacier basins in Wilkes-Queen Mary Land

Wei WANG¹, Yunzhong SHEN^{1*}, Qiujie CHEN¹, Fengwei WANG² & Yangkang YU¹

¹College of Surveying and Geo-informatics, Tongji University, Shanghai 200092, China

²State Key Laboratory of Marine Geology, Tongji University, Shanghai 200092, China

Received August 12, 2024; revised December 31, 2024; accepted January 22, 2025; published online March 19, 2025

Abstract To accurately evaluate the Antarctic Ice Sheet (AIS) mass change rate and its spatiotemporal characteristics, we derive the AIS mass change series from April 2002 to December 2023 using an improved point-mass model approach with data-driven regularization matrices and iteratively determined multiple regularization parameters. Then, we analyze the spatiotemporal characteristics of the mass change rate over the AIS, focusing on four glacier basins in the Wilkes Land-Queen Mary Land (WL-QML) region of the East AIS (EAIS), namely the Denman, Moscow, Totten, and Vincennes Bay glacier basins. The results indicate that the AIS contribution to GMSL (global mean sea level) rise peaked at 5.99 ± 0.43 mm in February 2020, followed by a mass gain period lasting over three years, ultimately resulting in a total GMSL contribution of 5.10 ± 0.52 mm by the end of 2023. Moreover, the AIS experienced substantial mass loss during the 2011–2020 period, with a rate of 142.06 ± 56.12 Gt a⁻¹, mainly due to intensified mass loss in the West AIS and the WL-QML region of the EAIS. Further analysis shows that the mass loss rate of the four glacier basins in the WL-QML region during the 2011–2020 period increased by 47.64 ± 8.14 Gt a⁻¹ compared with the 2002–2010 period, with expanded areas of mass loss spreading inland. Notably, the Vincennes Bay and Denman glacier basins transitioned from mass balance and accumulation to intense mass loss, respectively. An in-depth investigation reveals that the increased ice discharge and decreased SMB (surface mass balance) contribute 27.47% and 72.53%, respectively, to the intensified mass loss of the four glacier basins. Overall, the study presents the mass change characteristics of the AIS over the past 22 years, highlights the instability of four important glacier basins in the EAIS, and provides valuable scientific insights for related polar research.

Keywords Antarctic Ice Sheet, Mass change, Satellite gravimetry, Sea level change, Global climate change

Citation: Wang W, Shen Y, Chen Q, Wang F, Yu Y. 2025. Spatiotemporal mass change rate analysis from 2002 to 2023 over the Antarctic Ice Sheet and four glacier basins in Wilkes-Queen Mary Land. *Science China Earth Sciences*, 68, <https://doi.org/10.1007/s11430-024-1517-1>

1. Introduction

The Antarctic Ice Sheet (AIS) is a critical indicator of climate change and a significant contributor to global sea-level rise (Shepherd et al., 2018). Therefore, monitoring the mass changes over the AIS is essential for understanding global climate change given its significant impacts on coastal eco-

systems, human populations, and economic stability (Oppenheimer et al., 2019). Since 2002, the GRACE (Gravity Recovery and Climate Experiment) mission and its successor GRACE-FO (GRACE Follow-On) have provided unique observations for tracking the mass redistribution over the AIS (Tapley et al., 2019). Time-variable gravity field models derived from the GRACE/GRACE-FO (GRACE/-FO) mission have consistently estimated continent-wide, decadal-averaged mass balances, indicating ongoing mass loss in the

* Corresponding author (email: yzshen@tongji.edu.cn)

AIS (Schrama et al., 2014; Forsberg et al., 2017; Mu et al., 2017). For example, 95 ± 50 gigaton (Gt) a^{-1} for the 2002–2015 period (Forsberg et al., 2017), 89 ± 43 Gt a^{-1} for the 2002–2020 period (Groh and Horwath, 2021), and 144 ± 27 Gt a^{-1} for the 2011–2020 period (Willen et al., 2024). Most recently, the anomalously high precipitation over the AIS led to an unprecedented mass gain event between 2021 and 2022 (Wang et al., 2023a), raising the question of whether the AIS mass change in 2023 continues to accumulate or returns back to loss. To address this, it is imperative to answer this question by extending the AIS mass balance record, as it plays a vital role in predicting future sea level rise (Kopp et al., 2017).

In addition to monitoring the most recent status of the AIS mass balance, it is important to identify the specific regions where the ice mass loss occurs (Harig and Simons, 2015). The AIS covers approximately 14 million km^2 and it can be divided into three regions: the East AIS (EAIS), the West AIS (WAIS), and the Antarctic Peninsula Ice Sheet (APIS). Since the WAIS and the Antarctic Peninsula collectively contribute over 90% of the AIS mass loss (Shepherd et al., 2018), their mass change characteristics have attracted most of the research focus and have been well documented and analyzed (Sasgen et al., 2010; Lee et al., 2012; Su et al., 2018; Silva et al., 2020; Chuter et al., 2022; Yue et al., 2023). In contrast, the overall mass change of the EAIS has generally been estimated to be near balanced or even positive, which has resulted in relatively less scientific attention compared with the WAIS and the Antarctic Peninsula (Martín-Español et al., 2016; Gardner et al., 2018; Schröder et al., 2019; Shepherd et al., 2019; Smith et al., 2020; Stokes et al., 2022; Otosaka et al., 2023; Wang et al., 2023b). However, there are large drainage sectors in the EAIS, and if the entire EAIS completely melts there would be a global mean sea level (GMSL) rise of 52.2 ± 0.7 m (Morlighem et al., 2020). In Wilkes Land, Totten glacier has a GMSL rise potential of 3.9 m (Li et al., 2015) versus 3.3 m for the entire marine sector of WAIS (Bamber et al., 2009); the nearby Moscow glacier and Vincennes Bay's glaciers contain 1.3-m and 0.66-m GMSL rise potential, respectively (Rignot et al., 2019); in the Queen Mary Land, the Denman glacier holds an ice volume equivalent to a 1.5-m GMSL rise (Rignot et al., 2019; Miles et al., 2021).

Recent reports indicate that more glaciers in the EAIS are waking up (Qiu, 2017) and losing ice faster than anyone thought (Witze, 2018). In particular, with the vulnerability to enhanced mCDW (modified Circumpolar Deep Water) intrusion (Miles et al., 2016; Ribeiro et al., 2021), glaciers in Wilkes Land and Queen Mary Land have exhibited instability signs of ice thinning (Khazendar et al., 2013) and extensive grounding line retreat (Li et al., 2016; Shen et al., 2018; Picton et al., 2023) over the past two decades. This prompts the need to monitor, evaluate, and understand the

mass changes of these glacier basins. With the GRACE/-FO data, Velicogna et al. (2014, 2020) and Harig and Simons (2015) have observed mass loss signals over Wilkes Land; however, mass changes for individual glacier basins have not been estimated. Subsequently, Mohajerani et al. (2018) tried to qualify the glacier-basin-scale mass change of the Totten and Moscow glacier basins and reported a mass loss rate ranging from 14.6 ± 4.1 to 18.5 ± 6.6 Gt a^{-1} from April 2002 to August 2016. However, due to the limited spatial resolution of the large size of spherical caps near $3^\circ\times3^\circ$ used in Mohajerani et al. (2018), the mass changes of nearby glacier basins in Vincennes Bay are not separated, which brings uncertainty to the estimates of the Totten glacier basin and remaining mass changes of Vincennes Bay glacier basins unclear. Moreover, the mass change of the Denman glacier basin is still unclear at present.

With the updated GRACE/-FO data (Chen et al., 2023), we first generated a series of point-mass solutions over the AIS with higher spatial resolution and accuracy using an improved constrained point-mass model method (Wang et al., 2023b; Yu et al., 2024). Then, we estimated the long-term mass change rates over the AIS and the resulting GMSL contribution from April 2002 to December 2023. Furthermore, we analyzed the spatiotemporal characteristics of the AIS mass changes and emphasized mass changes of the less-studied but important glacier basins of Totten, Moscow, Denman, and Vincennes Bay in Wilkes-Queen Mary Land of the EAIS.

2. Study area, datasets and methodology

2.1 Study area

The AIS comprises 27 drainage basins (see Figure 1a). These basins are then grouped into three large regions according to Shepherd et al. (2018): the EAIS (Basins 2–17), the WAIS (Basins 1 and 18–23), and the APIS (Basins 24–27). This study mainly focuses on four glacier basins in Wilkes Land and Queen Mary Land, namely Denman, Moscow, Totten, and Vincennes Bay, and their locations are depicted in Figure 1b. The Denman, Moscow, Totten, and Vincennes Bay glacier basins cover an area of 265,529, 221,563, 555,995, and 134,874 km^2 , respectively. It should be noted that the areas of the Vanderfjord, Adams, Anza, Bond, and Underwood glacier basins are smaller than the native spatial resolution of GRACE/-FO (~300 km); therefore, they are regarded as an entity and referred to as “Vincennes Bay glacier basin”.

2.2 Datasets

To generate the point-mass solutions over the AIS, the GRACE/-FO monthly spherical harmonic coefficients, specifically the Tongji-Grace2022 data are used in this study.

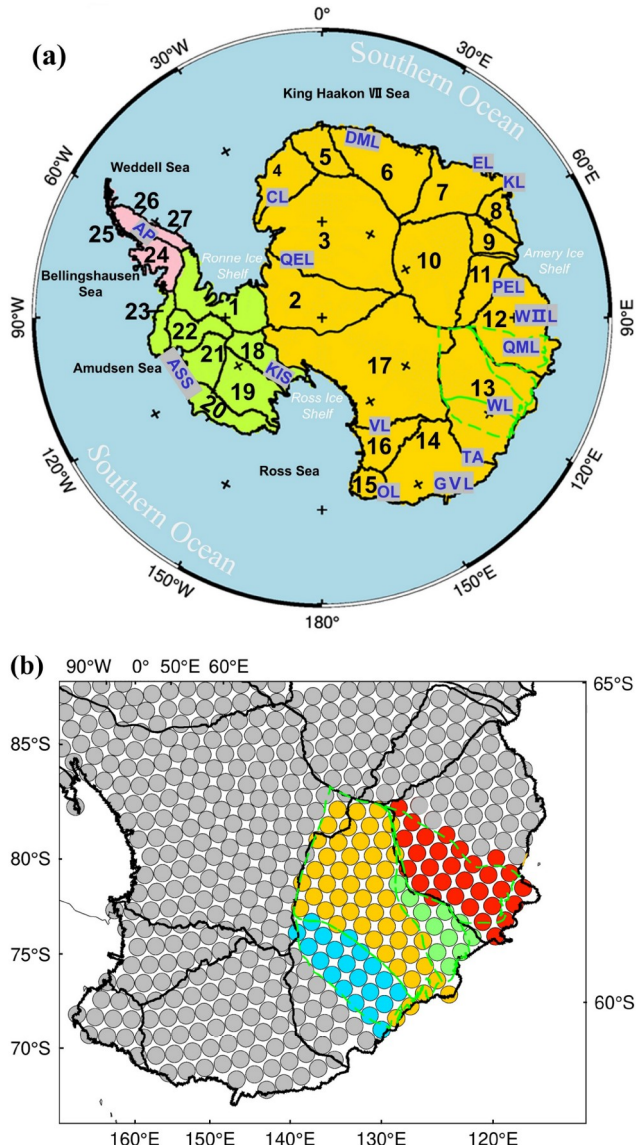


Figure 1 (a) Regional geographical distribution of basins 1–27; (b) a location map showing the Denman (red circles), Moscow (blue circles), Totten (orange circles), and Vincennes Bay (green circles) glacier basins along with the spatial distribution of point-mass positions. In (a), the EAIS, WAIS, and APIS are shown in orange, light green, and pink, respectively, and basin boundaries are obtained from <https://earth.gsfc.nasa.gov/cryo/data/polar-altimetry/antarctic-and-greenland-drainage-systems>; the land information is from <https://doi.org/10.1594/PANGAEA.951482>. QEL, Queen Elizabeth Land; CL, Coats Land; DML, Dronning Maud Land; EL, Enderby Land; KL, Kemp Land; PEL, Princess Elizabeth Land; WIL, Wilhelm II Land; QML, Queen Mary Land; WL, Wilkes Land; TA, Terre Adélie; GVL, George V Land; OL, Oates Land; VL, Victoria Land; KIS, Kamb Ice Stream; ASS, Amundsen Sea sector; AP, Antarctic Peninsula. In (b), green dashed lines indicate the boundary of glacier basins, the boundary data for these four glacier basins are obtained from <https://doi.org/10.5067/AXE4121732AD>.

This dataset is up to a degree/order of 96 and spans from April 2002 to December 2023 (with an 11-month gap from July 2017 to May 2018) (Chen et al., 2023). Since GRACE/-FO missions measure absolute gravity, the cumulative mass

change during the gap between GRACE and GRACE-FO can be determined with the first GARCE-FO and the last GRACE observations (Sasgen et al., 2020). Therefore, the data gap need not be filled in computing mass change rate. Since the Degree-1 coefficients are not measured in GRACE/-FO's center-of-mass frame, we added them back with those provided in Technical Note-13 (Sun et al., 2016). All C_{20} coefficients and C_{30} terms after August 2016 are replaced with corresponding values from Technical Note-14 (Loomis et al., 2019, 2020). The effect of GIA (glacial isostatic adjustment) is removed with the IJ05_R2 model (Ivins et al., 2013).

The Regional Atmospheric Climate Model Version 2.3p2 (RACMO2.3p2), with a spatial resolution of 27 km×27 km, is used to estimate the SMB (surface mass balance) over the AIS from January 2003 to December 2023 (van Wessem et al., 2018). RACMO2.3p2 combines the dynamics of the High-Resolution Limited Area Model (HIRLAM) (version 5.0.6; Undén et al., 2002) and the physics of the ECMWF-IFS (European Centre for Medium-Range Weather Forecasts-Integrated Forecasting System) (ECMWF, 2008). HIRLAM provides the best operational short-range forecasting system and solves explicit dynamical computations. The ECMWF-IFS models the physical processes and resolves the smaller-scale atmospheric processes through parameterization. The input data for these physical processes includes prognostic variables such as wind, temperature, humidity, cloud fraction, and liquid/ice water content. Consequently, relevant variables of SMB, such as precipitation, are derived from these outputs (van Wessem, 2016). The RACMO2.3p2 SMB and ice discharge from 2002 to 2023 for the Denman, Moscow, Totten, and Vincennes Bay glacier basins, as provided by Davison et al. (2023), are used to validate and interpret the observed mass changes by GRACE/-FO.

The monthly elevation change estimates over the AIS from satellite altimetry (Nilsson et al., 2022) for the 2002–2020 period are used to compare the spatial patterns of mass change rates derived from GRACE/-FO. The surface elevation changes (SEC) due to GIA and elastic solid earth rebound are corrected using the IJ05_R2 model (Ivins et al., 2013) with a scale factor of 1.0205 (Groh et al., 2012). Then, the SEC is converted to mass change using the method of Kuipers Munneke et al. (2015), in which the Institute for Marine and Atmospheric research Utrecht-Firm Densification Model (IMAU-FDM; Veldhuijsen et al., 2023) and RACMO2.3p2 are used (van Wessem et al., 2018).

2.3 Improved constrained point-mass model approach

To estimate monthly mass changes over the AIS, here we use the Improved Constrained Point-Mass Model (ICPM) approach developed based on that of Wang et al. (2023b). In

practice, we first set 2024 point-mass points of $1^\circ \times 1^\circ$ equal-area and 3616 pseudo-observations at the satellite altitude to cover both the AIS and its 600 km (about twice GRACE/-FO natural spatial resolution) buffer zone as in Wang et al. (2023b). Then, the design matrix is determined via Newton's law of gravitation, and ellipsoidal correction is considered (Ditmar, 2018). Considering that the observation equation is ill-conditioned, we constructed a series of data-driven regularization matrices to improve the spatial resolution of the solutions (Wang et al., 2024). The RMS (root mean square) of regularization matrices for point-mass over the buffer zone is set to 4 cm to correct for the land-to-ocean signal leakage. Finally, we derived the regularized solutions using iteratively determined multiple regularization parameters, i.e., iterative shrinking generalized ridge regression (IS-GRR) (e.g., Yu et al., 2024). The uncertainty of the point-mass solutions is evaluated using their MSE (mean squared error) in the constrained point-mass model.

Compared with the point-mass model proposed by Wang et al. (2023b), our approach introduces an improved method for determining the regularization matrix and regularization parameters. Specifically, while Wang et al. (2023b) employed a constant regularization matrix, we adopt a data-driven regularization matrix proposed by Wang et al. (2024), which is updated monthly based on GRACE observations. Furthermore, we introduce multiple parameter regularization proposed by Yu et al. (2024), whereas, Wang et al. (2023b) applied the Tikhonov regularization with a single regularization parameter for each observation equation (Tikhonov, 1963a, 1963b). The multiple parameter regularization can effectively balance signal retention and noise suppression across various spectral domains, outperforming the commonly used Tikhonov regularization (Yu et al., 2024). Further details of the ICPM approach are provided in Appendix (<https://link.springer.com>).

2.4 Mass change rate estimation

The mass change for a region is calculated by summing point-mass values at the ground within that region. The mass change rate for a given period is determined by least squares fitting to the time series of mass change $M(t)$ of a ground point-mass or a region, using the following equation:

$$M(t) = a + bt + A_1 \cos\left(\frac{2\pi}{T_1}t - \theta_1\right) + A_2 \cos\left(\frac{2\pi}{T_2}t - \theta_2\right), \quad T_1 = 1, \quad T_2 = \frac{1}{2}, \quad (1)$$

where a and b are the constant and mass change rate; the third and fourth terms on the right-hand side represent the annual and semi-annual signals, with A_1 , A_2 , θ_1 , and θ_2 denoting the annual, semi-annual amplitudes and phases; t is the time tag in years.

The uncertainty of the mass change rate at the 95% confidence level is derived as follows:

$$E_{\text{trend}} = 2\sqrt{\sigma_b^2 + \sigma_{\text{GIA}}^2}, \quad (2)$$

where σ_b denotes the fitting error of the mass change rate in eq. (1); σ_{GIA} is the standard deviation of the GIA model, which is empirically calculated through a multi-model comparison as described by Smith et al. (2020). This comparison includes six GIA models from Whitehouse et al. (2012), Ivins et al. (2013), A et al. (2013), Caron et al. (2018), Peltier et al. (2018), and Sasgen et al. (2018).

2.5 GMSL contribution estimate

In this study, we quantify the contribution of ice sheet mass changes to GMSL, which is determined based on the relationship that a 362.5-Gt mass variation corresponds to a 1-mm GMSL change (Cogley, 2012). A negative mass change for a given region indicates a loss of land mass in Gt, and the corresponding increase in ocean mass is expressed in mm GMSL. Therefore, the mass change rate for a region is expressed in Gt a^{-1} , while the corresponding GMSL change is measured in mm a^{-1} .

The contribution to GMSL can be derived by the following equation:

$$h_{\text{GMSL}} = -\frac{m_{\text{ice}}}{\rho_w s_{\text{ocean}}}, \quad (3)$$

where m_{ice} denotes the ice mass change in Gt; ρ_w is the density of water, typically assumed to be the density of freshwater ($1 \times 10^3 \text{ kg km}^{-3}$), as used in Blazquez (2020); s_{ocean} represents the area of the global ocean, approximately $362.5 \times 10^6 \text{ km}^2$ (Cogley, 2012).

Then, the relevant values are substituted into eq. (3), and the GMSL contribution can be directly estimated using the following formula:

$$h_{\text{GMSL}} = -\frac{m_{\text{ice}}}{362.5}, \quad (4)$$

in which the unit of mass change m_{ice} is Gt (Gt a^{-1} for its rate) and that of the GMSL contribution h_{GMSL} is mm (mm a^{-1} for its rate).

3. Results and analysis

3.1 Long-term and interannual mass change from 2002 to 2023

Figure 2a shows the spatial distribution of mass change rates over the AIS from April 2002 to December 2023, with seven regions of significant mass change rates labeled. In Figure 2b, the mass change time series and the resulting GMSL change of the seven regions and the AIS are plotted.

The mass change estimates exhibit considerable spatial

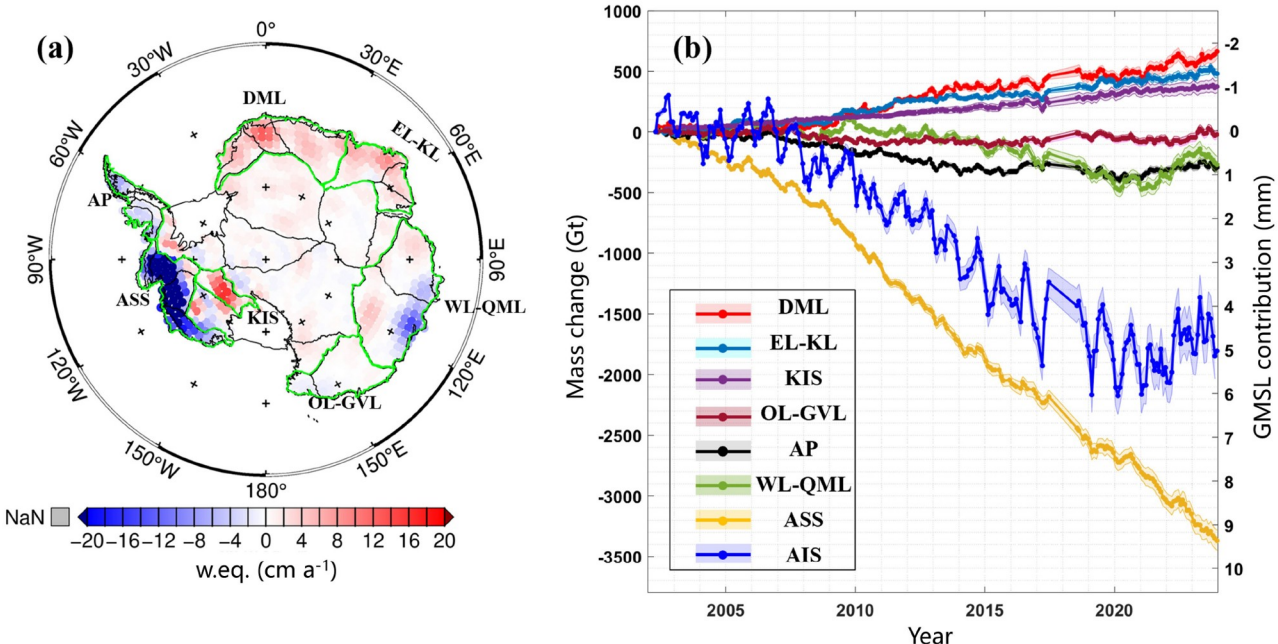


Figure 2 (a) Spatial distribution of mass change rates over the AIS from April 2002 to December 2023. The unit “w.eq.” is short for “water-equivalent”. The boundaries of the seven regions are shown in green solid lines. DML, Dronning Maud Land; EL-KL, Enderby Land and Kemp Land; KIS, Kamb Ice Stream; OL-GVL, Oates Land and George V Land; AP, Antarctic Peninsula; WL-QML, Wilkes Land and Queen Mary Land; ASS, Amundsen Sea sector. (b) Mass change time series for the seven regions and the AIS with the gap between GRACE and GRACE-FO shown in grey shadow.

variation across the coastal AIS, with distinct mass loss and gain signals during the study period. Specifically, the Amundsen Sea sector (ASS) in WAIS stands out with the largest-magnitude mass loss of 3364.40 ± 174.60 Gt (equivalent to 9.28 ± 0.48 mm GMSL rise contribution) during the study period. The Wilkes Land (WL) and neighboring Queen Mary Land (QML) in the EAIS also show a notable mass loss rate. Although much less than that of the ASS, the WL-QML is the second largest GMSL contributor of the AIS before an unprecedented surface mass accumulation around 2020 (Wang et al., 2023a), it cumulatively contributed 482.13 ± 54.38 Gt (equivalent to 1.33 ± 0.15 mm GMSL rise contribution) from April 2002 to February 2020. Additionally, the coastal regions of Oates Land and George V Land (OL-GVL) show a slight mass loss signal. However, this region makes almost negligible contributions to GMSL at present, because the mass gain in the second decade offsets the loss in the first decade of the 21st century. In contrast, the Kamb Ice Stream (KIS) has gained mass in the study period, associated with long-term thickening and reduced ice stream flow velocities (Pritchard et al., 2009; Pritchard et al., 2012). Dronning Maud Land (DML) and Enderby Land (EL) exhibit clear mass gain rates, particularly in the years 2009, 2011, and 2021–2022 when intense snowfall events occurred (Boening et al., 2012; Wang et al., 2023a). Overall, the spatial distribution of long-term mass change rates generally agrees with that recovered by previous studies from GRACE/-FO data (Velicogna et al., 2020; Groh and Horwath, 2021) but adds more spatial variability and details, such as the slight mass loss around the KIS and the mass gain over Basin 1. These additional signals benefit from the higher degree/order GRACE/-FO data that contain more observation information and the constrained point-mass method that improves the spatial resolution of the estimates. These additional signals can be confirmed with those in high-resolution elevation change maps from satellite radar altimetry, such as those in Figure 2 of Shepherd et al. (2019).

We present the mass change series and resulting GMSL contributions for the entire AIS from April 2002 to December 2023 in Figure 3. The AIS mass changes show a long-term mass loss rate with significant interannual variability. Based on previous findings indicating that the AIS mass changed around the years 2010 and 2020 (Nilsson et al., 2022; Wang et al., 2023b), we divide the mass change time series into three periods, i.e., the first decade of the 21st century (roughly 2002–2010), the second decade (2011–2020), and the beginning of the third decade (2021–2023) and estimate the mass change rates for three corresponding periods. Moreover, we map the spatial distributions of mass change rates and show the regional mass loss rates of seven regions in Figure 4. Here, we calculate the AIS mass change rate from 2002 to 2023 as -111.13 ± 55.58 Gt a^{-1} , which is slightly lower than the rate from 2002 to 2020, due to a mass gain (107.79 ± 74.90 Gt a^{-1}) from 2021 to 2023. Figure 3 indicates that during the study period, the AIS cumulatively contributed the most to the GMSL rise of 5.99 ± 0.43 mm in

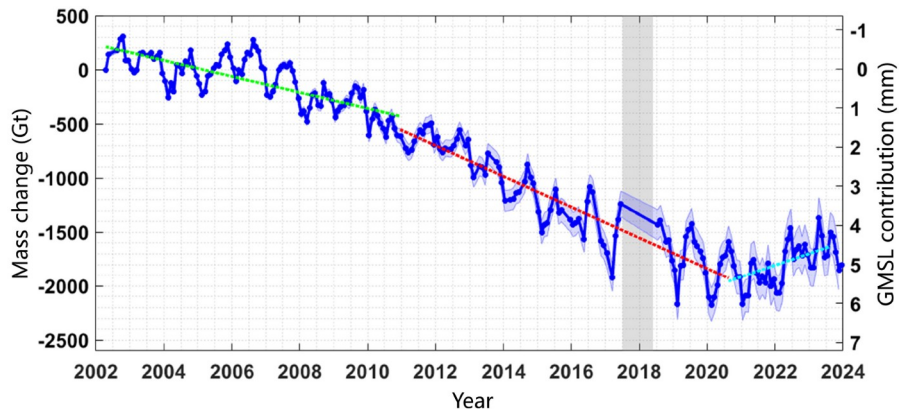


Figure 3 Mass change series for the AIS from April 2002 to December 2023. The grey shadow shows the gap between GRACE and GRACE-FO.

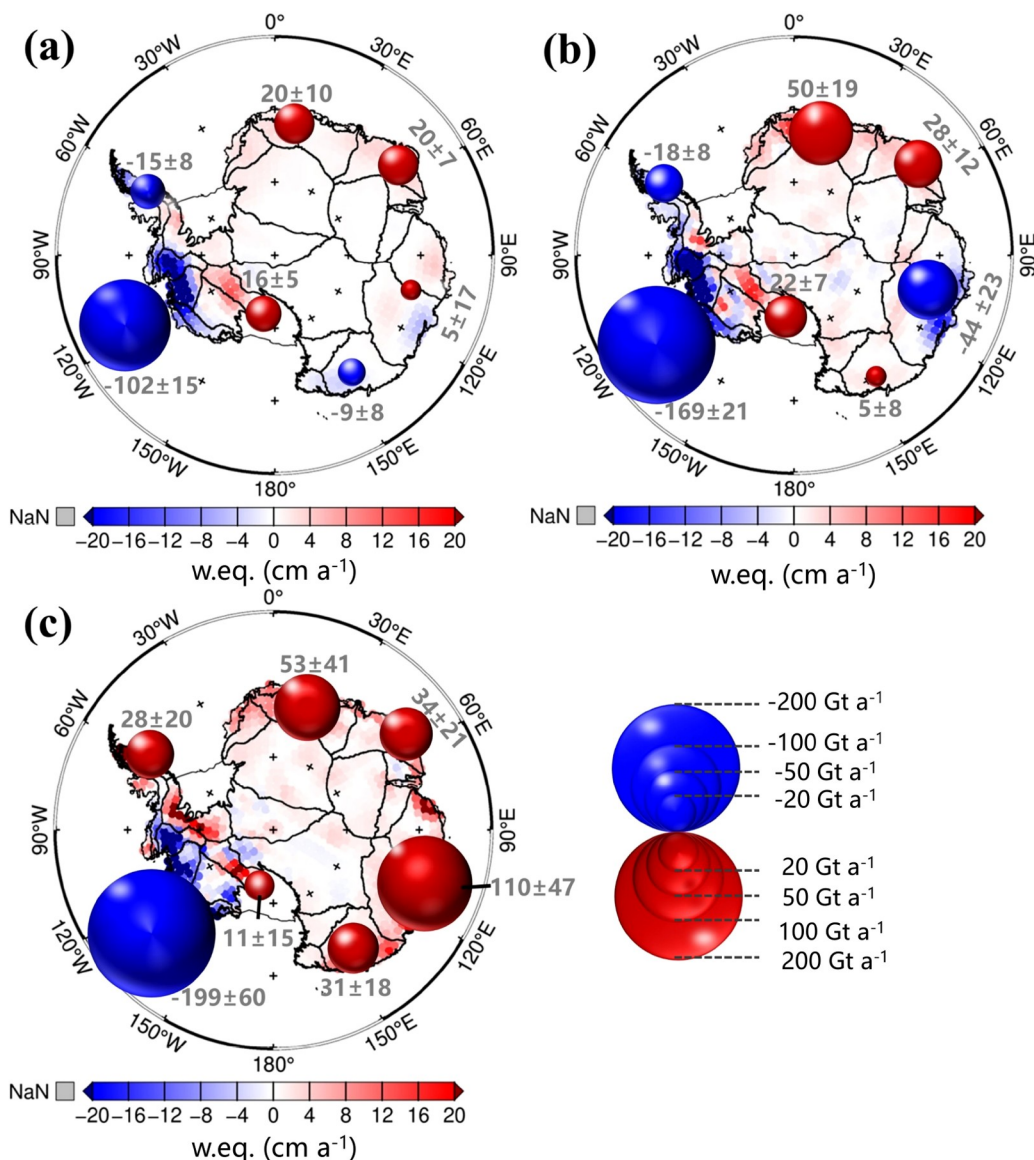


Figure 4 Spatial distributions of mass change rates over the AIS and seven important regions for three sub-periods of 2002–2010 (a), 2011–2020 (b), and 2021–2023 (c).

February 2020. Following a three-year period of mass gain, the AIS cumulatively contributed 5.10 ± 0.52 mm to the GMSL rise from April 2002 to December 2023.

The mass change rate from 2002 to 2020 is -120.23 ± 55.64 Gt a $^{-1}$, falling within the error range of other recent studies with GRACE/-FO data, such as -90.9 ± 43.5 Gt a $^{-1}$ from April 2002 to July 2020 (Groh and Horwath, 2021) and -126 ± 9 Gt a $^{-1}$ from April 2002 to August 2019 (Loomis et al., 2020). Moreover, our estimate agrees well with the IOM (Input-Output Method) result of -89 ± 99 Gt a $^{-1}$ from 2000 to 2020 (Yang et al., 2023) and a satellite altimetry result of ~ 118 Gt a $^{-1}$ from 2003 to 2019 (Smith et al., 2020). Notably, our findings reveal that the mass loss rate in the second decade of the 21st century (142.06 ± 56.12 Gt a $^{-1}$) is twice that in the first decade (73.79 ± 56.27 Gt a $^{-1}$). Furthermore, the mass loss rate estimate of the AIS from 2011 to 2020 is generally consistent with the result derived from satellite altimetry of Schröder et al. (2019), which is 137 ± 25 Gt a $^{-1}$ from 2010 to 2017. Moreover, from Figure 4a and 4b, it is evident that the intensity of mass loss primarily originated from the ASS and WL-QML. Specifically, the mass loss rate of ASS is intensified from 102 ± 15 to 169 ± 21 Gt a $^{-1}$ associated with accelerated grounding line retreat in the Pine Island and Thwaites glaciers (Davison et al., 2023). Meanwhile, the WL-QML region shows a notable shift from a slight mass gain to a severe loss, which highlights the importance of monitoring the stability of glaciers in this region of the EAIS. Further details are provided in Section 3.2.

3.2 Intense mass loss over Wilkes Land and Queen Mary Land in East Antarctica

Focusing on the intense mass loss over Wilkes Land and Queen Mary Land in East Antarctica, we compute the mass change time series for four key glacier basins in this region—Denman, Moscow, Totten, and Vincennes Bay, and estimate their mass change rates for the periods of 2002–2010 and 2011–2020. The results are presented in Figure 5. The four glacier basins exhibit long-term mass loss signals, accompanied by seasonal and interannual variability. The mass change rate for the Denman glacier basin shifted from a state of mass accumulation (5.44 ± 2.88 Gt a $^{-1}$) for the period 2002–2010 to a intense mass loss with a change rate of -14.32 ± 2.90 Gt a $^{-1}$ for the period 2011–2020. The mass change rate of the Moscow glacier basin is -5.56 ± 2.87 Gt a $^{-1}$ for 2011–2020, nearly three times the rate for the period 2002–2010. Besides, the mass loss rate of the Totten glacier basin increased from 6.35 ± 2.94 Gt a $^{-1}$ during the period 2002–2010 to 19.90 ± 2.88 Gt a $^{-1}$ during the period 2011–2020, which generally agrees with the finding in Harig and Simons (2015) that the Totten glacier basin has experienced local mass loss and acceleration from 2003 to 2014. Most strikingly, the Vincennes Bay glacier basin was relatively

stable for the first decade but started to show a significant mass change from its original state after 2010, and its mass change rate reached -10.92 ± 2.84 Gt a $^{-1}$ during the period 2011–2022. The intense mass loss of the Denman, Moscow, Totten, and Vincennes Bay glacier basins contribute to a GMSL rise of 0.14 ± 0.03 mm a $^{-1}$ during the period 2011–2022.

Previously, McMillan et al. (2014) reported a mass loss rate of 10 ± 3 Gt a $^{-1}$ for the Totten glacier basin between 2010 and 2013 with satellite altimetry data; and Li et al. (2016) documented a mass loss rate of 6.8 ± 2.4 Gt a $^{-1}$ from 1989 to 2015 with the IOM. Both values are consistent with our estimate for the first period despite the differences in time-span. However, their results are less than ours for the period 2011–2020, indicating that the mass loss of the Totten glacier basin is more severe than previously reported. Moreover, using GRACE/-FO data, a prior work of Harig and Simons (2015) estimated a mass loss of 17 ± 4 Gt a $^{-1}$ during the period 2003–2014 for a large region clockwise from QML to OL-GVL, and Mohajerani et al. (2018) reported that the Moscow and Totten glacier basins, including Vincennes Bay glacier basin, have a total mass loss rate ranging from 14.6 ± 4.1 to 18.5 ± 6.6 Gt a $^{-1}$ from 2002 to 2016. In this study, our analysis complements previous work by showing mass change rates of individual glacier basins within the WL-QML region for two periods as shown in Figure 5. Besides, we provide new findings that the four studied glacier basins have a total mass loss rate of 3.06 ± 5.77 Gt a $^{-1}$ for the period 2002–2010 while the mass loss rate reaches 50.70 ± 5.74 Gt a $^{-1}$ for the period 2011–2020, suggesting an intensified mass loss over the WL-QML region. The findings coincide with the previous findings from independent observations of satellite altimetry that WL-QML has been showing accelerating negative elevation change since 2010 (Nilsson et al., 2022).

To further analyze the mass change characteristics of these four glacier basins, we map the mass change rates for the periods 2002–2010 and 2011–2020, as well as the difference between the two periods in Figure 6a, 6c, and 6e. Additionally, we provide corresponding mass change rate estimates from satellite altimetry for comparison, as shown in Figure 6b, 6d, and 6f. It can be observed that results from both GRACE/-FO and satellite altimetry indicate glacier mass loss in Wilkes Land during the 2002–2010 and 2011–2020 periods. The mass loss signals are enhanced in the period 2010–2020, with expanded areas spreading inland and increased magnitude. For the Denman glacier basin, GRACE results suggest a weak mass gain during the period 2002–2010, whereas satellite altimetry indicates both mass gain and loss signals. This may be attributed to the uncertainty associated with the conversion from elevation change to mass change, since the elevation changes for a similar period, as shown in Figure 2 by Shepherd et al. (2019), are

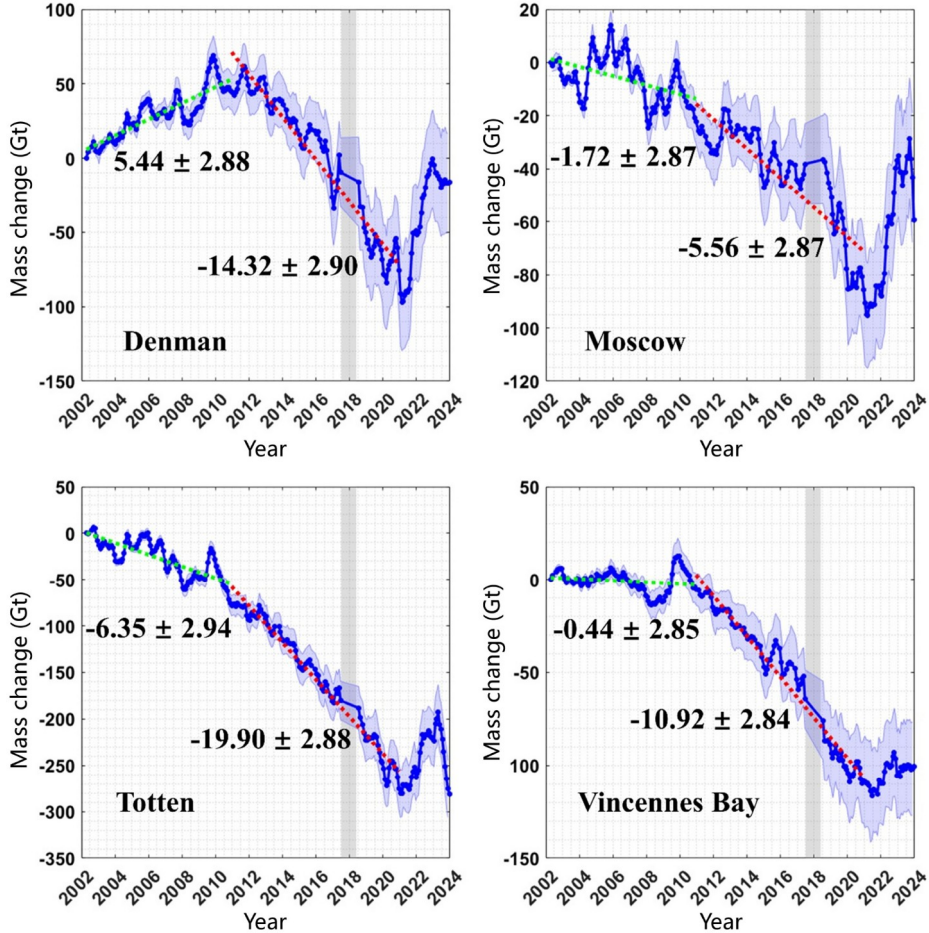


Figure 5 Mass change series for the Denman, Moscow, Totten, and Vincennes Bay glacier basins from April 2002 to December 2023. The unit of the mass change rate is Gt a^{-1} , and the grey shadow shows the gap between GRACE and GRACE-FO missions.

mostly positive over the Denman glacier basin. During the period 2011–2020, both GRACE/-FO and satellite altimetry results indicate a significant mass loss rate for these four glacier basins. Furthermore, Figure 6e and 6f suggest a noticeable intensification of glacier mass loss rate for the Denman, Moscow, Totten, and Vincennes Bay glacier basins in this period.

4. Discussion

To reveal the direct driving factors of the mass change of the Denman, Moscow, Totten, and Vincennes Bay glacier basins, we present the annual variations in SMB, ice discharge at the grounding line (Discharge), and glacier-basin-scale net annual mass changes (or mass balance), derived from the IOM (SMB minus Discharge) in Figure 7. SMB uncertainty is calculated assuming a 6.1% uncertainty in monthly values, as used in Li et al. (2016) and Mohajerani et al. (2018). Since SMB variation is dominant by the sum of the total precipitation (snowfall plus rain) and sublimation (Bodart and

Bingham, 2019), we also show the spatial distributions of mean total precipitation and sublimation for the periods 2002–2010 and 2011–2020, along with the corresponding differences in Figure 8a–8f.

The differences between the mass loss rates for the periods 2002–2010 and 2011–2020 from GRACE/-FO data are $-19.76 \pm 4.08 \text{ Gt a}^{-1}$ for the Denman, $-3.84 \pm 4.06 \text{ Gt a}^{-1}$ for the Moscow, $-13.56 \pm 4.11 \text{ Gt a}^{-1}$ for the Totten, and $-10.49 \pm 4.03 \text{ Gt a}^{-1}$ for the Vincennes Bay glacier basin. These values are consistent with those from the IOM within their uncertainties (see Figure 7). The annual mass loss for these four glacier basins occurs when SMB falls below discharge, and the increased ice discharge and decreased SMB are attributed to the observed intensification of mass loss. Overall, for the four glacier basins, ice discharge increased by $8.96 \pm 14.59 \text{ Gt a}^{-1}$, while SMB decreased by $23.65 \pm 27.53 \text{ Gt a}^{-1}$ from the 2002–2010 period to the 2011–2020 period. This indicates that ice discharge and SMB account for 27.47% and 72.53% of the mass loss intensification, respectively. Figure 8 shows that the accelerated mass loss in WL-QML during the period 2011–2020 is mainly attributed to the anomalous

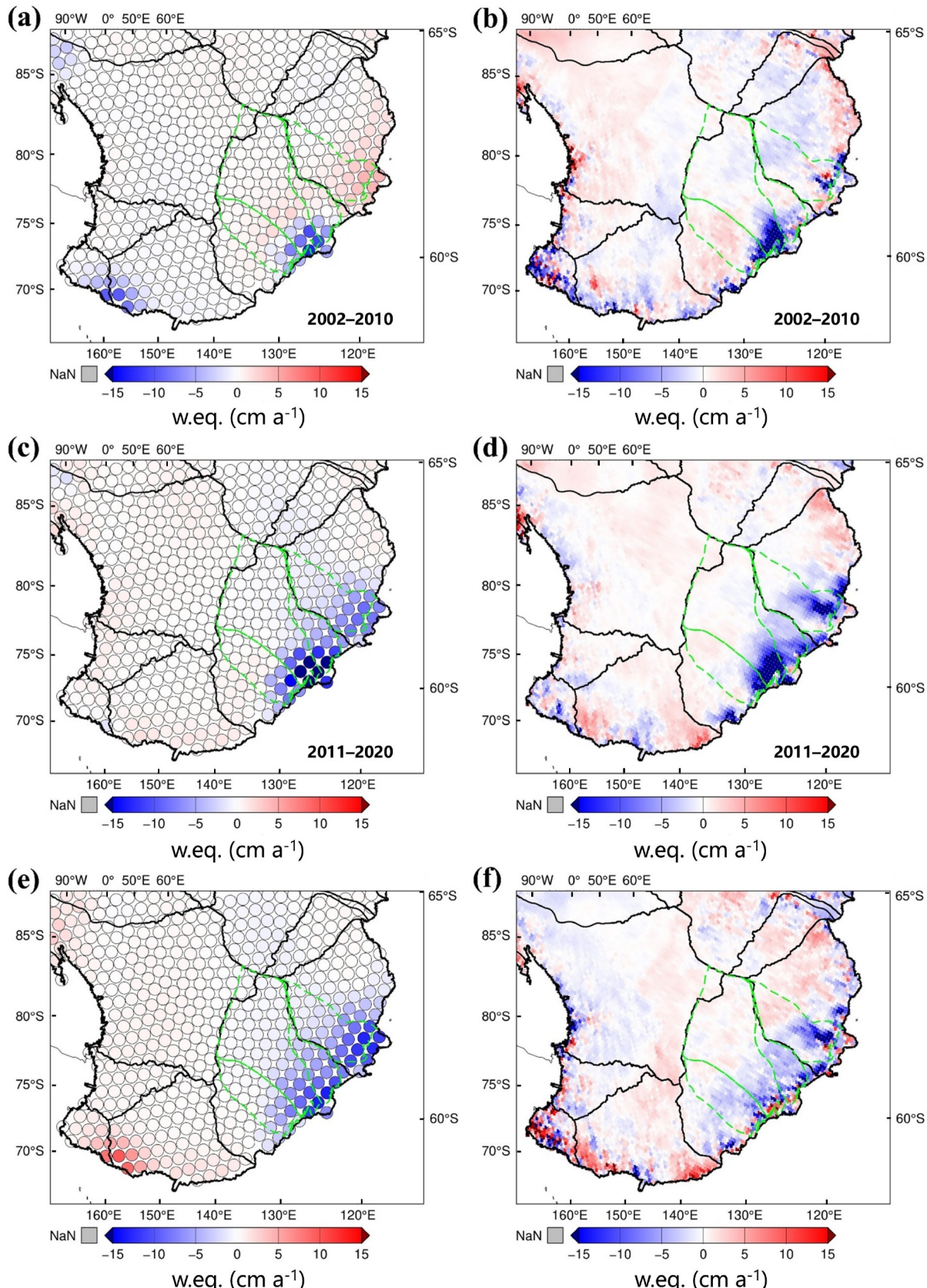


Figure 6 Spatial distribution of mass change rates for different periods and the corresponding differences. (e) is derived from (c) minus (a), and (f) is derived from (d) minus (b), the left column is derived from GRACE-FO, while the right is derived from satellite altimetry, the green dashed lines show the boundary of the Denman, Moscow, Totten, and Vincennes Bay glacier basins.

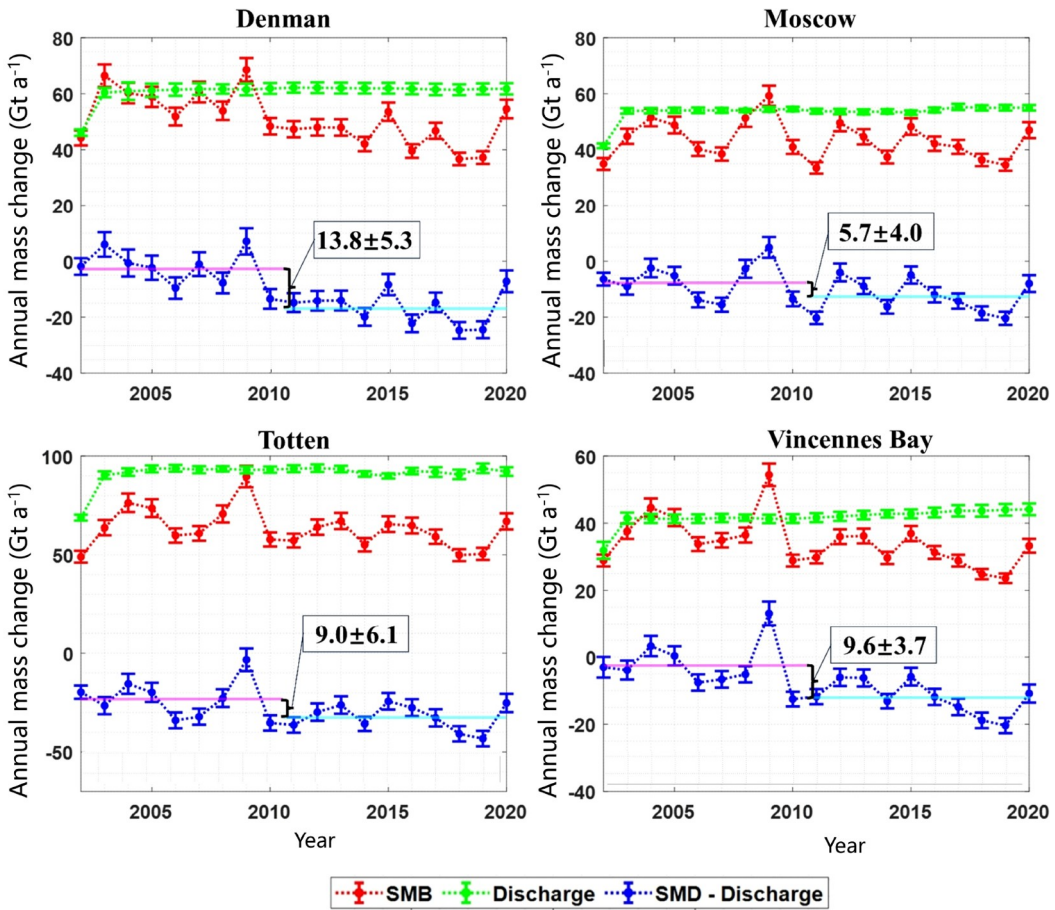


Figure 7 Annual SMB, ice discharge, and net mass changes for the Denman, Moscow, Totten, and Vincennes Bay glacier basins for the period 2002–2020. The pink line shows the mean mass change for the period 2002–2010, while the cyan line corresponds to the period 2011–2020, the differences in mass change between the two periods are labeled in the rectangular boxes (unit is Gt a^{-1}).

reduction in precipitation. In other words, the substantial decrease in precipitation has resulted in a larger disparity between the ice discharge loss and SMB accumulation in this region. Moreover, the spatial distribution of the precipitation reduction coincides with the reduction of mass loss, highlighting the role of precipitation in modulating the mass changes over the WL-QML region (Kim et al., 2020).

5. Conclusion

In this study, we provide an extensive record of AIS mass change from April 2002 to December 2023 and analyze the corresponding spatiotemporal characteristics. Our investigation reveals that the previously reported record-breaking mass gain of the AIS between the years 2021 and 2022 has continued through the year 2023, persisting for the past three years from 2021 to 2023. Consequently, the AIS has contributed negatively to the GMSL rise for the past three years, and its total contribution to the GMSL rise was reduced to $5.10\pm0.52 \text{ mm}$ from April 2002 to December 2023. Moreover, our analysis shows that AIS mass loss was

the most substantial during the second decade of the 21st century. During this period, there was an increasing rate of mass loss within the ASS and an intensification of mass loss in the WL-QML regions of the EAIS, with mass loss in larger areas spreading inland and a higher magnitude of loss. Specifically, the mass loss rate for four glacier basins of the Denman, Moscow, Totten, and Vincennes Bay glacier basins in the WL-QML region increased from $3.06\pm5.77 \text{ Gt a}^{-1}$ for the period 2002–2010 to $50.70\pm5.74 \text{ Gt a}^{-1}$ for the period 2011–2020. The observed intensification of mass loss for the four glacier basins is attributed to the increased ice discharge and decreased SMB, with ice discharge and SMB contributing 27.47% and 72.53%, respectively.

Our study provides the latest insights into the mass change rates of the AIS, serving as a foundation for predicting future AIS mass evolution and consequent impact on GMSL rise. Furthermore, we present multiple lines of evidence from GRACE-FO, satellite altimetry, and the IOM for the intense instability of the Denman, Moscow, Totten, and Vincennes Bay glacier basins in East Antarctica. Notably, the Denman glacier basin, previously less studied by the scientific community, has transitioned from a slight mass gain to a sig-

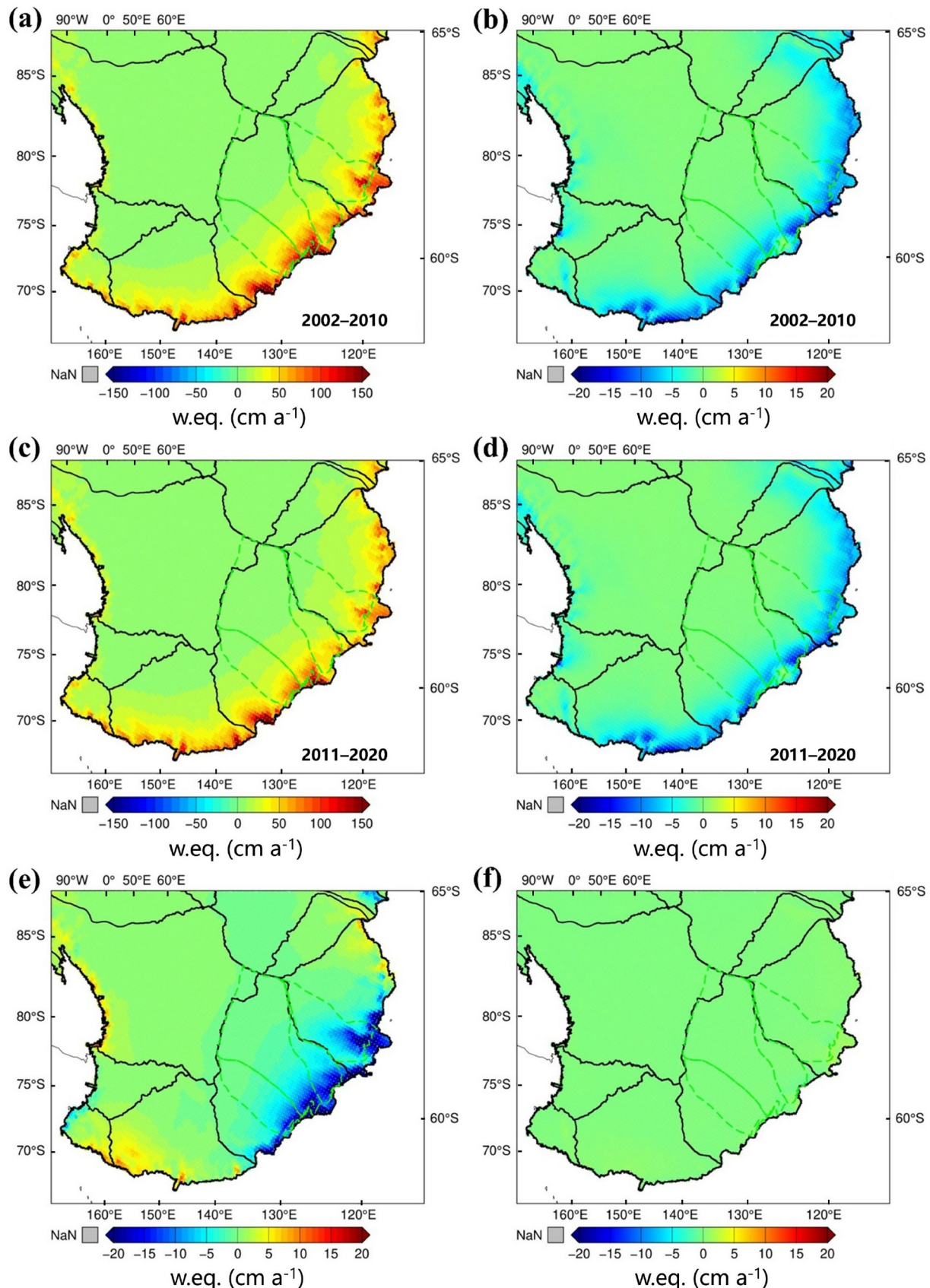


Figure 8 Spatial distribution of mean precipitation (a, c) and sublimation (b, d), along with the corresponding differences (e, f) in different periods. (e) is derived from (c) minus (a) and (f) is derived from (d) minus (b).

nificant mass loss state. The scientific community should pay more attention to these coastal glacier basins in East Antarctica with a multimeter GMSL rise potential, as this aspect bears significant implications for addressing global climate change.

Acknowledgements Dr. Michiel van den Broeke and Dr. Sanne B.M. Veldhuisen are acknowledged for providing the RACMO2.3p2 and IMAU-FDM data, respectively. This work was supported by the National Natural Science Foundation of China (Grant Nos. 42394131 & 42274005).

Conflict of interest The authors declare that they have no conflict of interest.

References

- A G, Wahr J, Zhong S J. 2013. Computations of the viscoelastic response of a 3-D compressible Earth to surface loading: An application to Glacial Isostatic Adjustment in Antarctica and Canada. *Geophys J Int*, 192: 557–572
- Bamber J L, Riva R E M, Vermeersen B L A, LeBrocq A M. 2009. Reassessment of the potential sea-level rise from a collapse of the West Antarctic Ice Sheet. *Science*, 324: 901–903
- Blazquez A. 2020. Satellite characterization of water mass exchange between ocean and continents at interannual to decadal timescales. Dissertation for Doctoral Degree. Toulouse: Université Toulouse III-Paul Sabatier
- Bodart J A, Bingham R J. 2019. The impact of the extreme 2015–2016 El Niño on the mass balance of the Antarctic Ice Sheet. *Geophys Res Lett*, 46: 13862–13871
- Boening C, Lebsack M, Landerer F, Stephens G. 2012. Snowfall-driven mass change on the East Antarctic ice sheet. *Geophys Res Lett*, 39: 2012GL053316
- Caron L, Ivins E R, Larour E, Adhikari S, Nilsson J, Blewitt G. 2018. GIA model statistics for GRACE hydrology, cryosphere, and ocean science. *Geophys Res Lett*, 45: 2203–2212
- Chen Q J, Shen Z L, Shen YZ, Chen W, Zhang XF. 2023. Tongji-GRACE2022: New global temporal Earth's gravity field models derived from k-band and Iri inter-satellite rang-rate data. In: XXVIII General Assembly of the International Union of Geodesy and Geophysics (IUGG). Berlin
- Chuter S J, Zammit-Mangion A, Rougier J, Dawson G, Bamber J L. 2022. Mass evolution of the Antarctic Peninsula over the last 2 decades from a joint Bayesian inversion. *Cryosphere*, 16: 1349–1367
- Cogley J G. 2012. Area of the ocean. *Mar Geod*, 35: 379–388
- Davison B J, Hogg A E, Slater T, Rigby R. 2023. Antarctic Ice Sheet grounding line discharge from 1996 through 2023. *Earth Syst Sci Data Discuss*, 2023: 1–35
- Ditmar P. 2018. Conversion of time-varying Stokes coefficients into mass anomalies at the Earth's surface considering the Earth's oblateness. *J Geod*, 92: 1401–1412
- ECMWF. 2008. IFS Documentation: Part IV: Physical processes (CY33R1). Technical Report. ECMWF
- Forsberg R, Sørensen L, Simonsen S. 2017. Greenland and Antarctica Ice Sheet mass changes and effects on global sea level. *Surv Geophys*, 38: 89–104
- Gardner A S, Moholdt G, Scambos T, Fahnestock M, Ligtenberg S, van den Broeke M, Nilsson J. 2018. Increased West Antarctic and unchanged East Antarctic ice discharge over the last 7 years. *Cryosphere*, 12: 521–547
- Groh A, Horwath M. 2021. Antarctic Ice Mass change products from GRACE/GRACE-FO using tailored sensitivity kernels. *Remote Sens*, 13: 1736
- Groh A, Ewert H, Scheinert M, Fritsche M, Rülke A, Richter A, Rosenau R, Dietrich R. 2012. An investigation of Glacial Isostatic Adjustment over the Amundsen Sea sector, West Antarctica. *Glob Planet Change*, 98–99: 45–53
- Harig C, Simons F J. 2015. Accelerated West Antarctic ice mass loss continues to outpace East Antarctic gains. *Earth Planet Sci Lett*, 415: 134–141
- Ivins E R, James T S, Wahr J, Schrama E J O, Landerer F W, Simon K M. 2013. Antarctic contribution to sea level rise observed by GRACE with improved GIA correction. *J Geophys Res-Solid Earth*, 118: 3126–3141
- Khazendar A, Schodlok M P, Fenty I, Ligtenberg S R M, Rignot E, van den Broeke M R. 2013. Observed thinning of Totten Glacier is linked to coastal polynya variability. *Nat Commun*, 4: 9
- Kim B H, Seo K W, Eom J, Chen J, Wilson C R. 2020. Antarctic ice mass variations from 1979 to 2017 driven by anomalous precipitation accumulation. *Sci Rep*, 10: 20366
- Kopp R E, DeConto R M, Bader D A, Hay C C, Horton R M, Kulp S, Oppenheimer M, Pollard D, Strauss B H. 2017. Evolving understanding of Antarctic Ice-Sheet physics and ambiguity in probabilistic sea-level projections. *Earth's Future*, 5: 1217–1233
- Kuipers Munneke P, Ligtenberg S R M, Noël B P Y, Howat I M, Box J E, Mosley-Thompson E, McConnell J R, Steffen K, Harper J T, Das S B, van den Broeke M R. 2015. Elevation change of the Greenland Ice Sheet due to surface mass balance and firn processes, 1960–2014. *Cryosphere*, 9: 2009–2025
- Lee H, Shum C K, Howat I M, Monaghan A, Ahn Y, Duan J, Guo J Y, Kuo C Y, Wang L. 2012. Continuously accelerating ice loss over Amundsen Sea catchment, West Antarctica, revealed by integrating altimetry and GRACE data. *Earth Planet Sci Lett*, 321–322: 74–80
- Li X, Rignot E, Morlighem M, Mouginot J, Scheuchl B. 2015. Grounding line retreat of Totten Glacier, East Antarctica, 1996 to 2013. *Geophys Res Lett*, 42: 8049–8056
- Li X, Rignot E, Mouginot J, Scheuchl B. 2016. Ice flow dynamics and mass loss of Totten Glacier, East Antarctica, from 1989 to 2015. *Geophys Res Lett*, 43: 6366–6373
- Loomis B D, Rachlin K E, Luthcke S B. 2019. Improved Earth oblateness rate reveals increased ice sheet losses and mass-driven sea level rise. *Geophys Res Lett*, 46: 6910–6917
- Loomis B D, Rachlin K E, Wiese D N, Landerer F W, Luthcke S B. 2020. Replacing GRACE/GRACE-FO C_{30} with satellite laser ranging: Impacts on Antarctic Ice Sheet mass change. *Geophys Res Lett*, 47: 7
- Martín-Español A, Zammit-Mangion A, Clarke P J, Flament T, Helm V, King M A, Luthcke S B, Petrie E, Rémy F, Schön N, Wouters B, Bamber J L. 2016. Spatial and temporal Antarctic Ice Sheet mass trends, glacio-isostatic adjustment, and surface processes from a joint inversion of satellite altimeter, gravity, and GPS data. *J Geophys Res-Earth Surf*, 121: 182–200
- McMillan M, Shepherd A, Sundal A, Briggs K, Muir A, Ridout A, Hogg A, Wingham D. 2014. Increased ice losses from Antarctica detected by CryoSat-2. *Geophys Res Lett*, 41: 3899–3905
- Miles B W J, Stokes C R, Jamieson S S R. 2016. Pan-ice-sheet glacier terminus change in East Antarctica reveals sensitivity of Wilkes Land to sea-ice changes. *Sci Adv*, 2: e1501350
- Miles B W J, Jordan J R, Stokes C R, Jamieson S S R, Hilmar Gudmundsson G, Jenkins A. 2021. Recent acceleration of Denman Glacier (1972–2017), East Antarctica, driven by grounding line retreat and changes in ice tongue configuration. *Cryosphere*, 15: 663–676
- Mohajerani Y, Velicogna I, Rignot E. 2018. Mass loss of Totten and Moscow University Glaciers, East Antarctica, using regionally optimized GRACE mascons. *Geophys Res Lett*, 45: 7010–7018
- Morlighem M, Rignot E, Binder T, Blankenship D, Drews R, Eagles G, Eisen O, Ferraccioli F, Forsberg R, Fretwell P, Goel V, Greenbaum J S, Gudmundsson H, Guo J, Helm V, Hofstede C, Howat I, Humbert A, Jakob W, Karlsson N B, Lee W S, Matsuoka K, Millan R, Mouginot J, Paden J, Pattyn F, Roberts J, Rosier S, Ruppel A, Seroussi H, Smith E C, Steinhage D, Sun B, Broeke M R, Ommen T D, Wessem M, Young D A. 2020. Deep glacial troughs and stabilizing ridges unveiled beneath the margins of the Antarctic ice sheet. *Nat Geosci*, 13: 132–137

- Mu D P, Yan H M, Feng W, Peng P. 2017. GRACE leakage error correction with regularization technique: Case studies in Greenland and Antarctica. *Geophys J Int*, 208: 1775–1786
- Nilsson J, Gardner A S, Paolo F S. 2022. Elevation change of the Antarctic Ice Sheet: 1985 to 2020. *Earth Syst Sci Data*, 14: 3573–3598
- Oppenheimer M, Glavovic B C, Hinke J, van de Wal R, Magnan A K, Abd-Elgawad A, Ca R, Cifuentes-Jara M, DeConto R M, Ghosh T, Hay I, Isla F, Marzeion B, Meysignac B, Sebesvari Z. 2019. Sea level rise and implications for low-lying islands, coasts and communities. In: Pörtner H O, Roberts D C, Masson-Delmontte V, Zhai P, Tignor M, Poloczanska E, Mintenbeck K, Alegria A, Nicolai M, Okem A, Petzold J, Rama B, Weyer N M, eds. *IPCC Special Report on the Ocean and Cryosphere in a Changing Climate*. Cambridge: Cambridge University Press. 321–445
- Otosaka I N, Horwath M, Mottram R, Nowicki S. 2023. Mass balances of the Antarctic and Greenland Ice Sheets monitored from space. *Surv Geophys*, 44: 1615–1652
- Pictor H J, Stokes C R, Jamieson S S R, Floricioiu D, Krieger L. 2023. Extensive and anomalous grounding line retreat at Vanderford Glacier, Vincennes Bay, Wilkes Land, East Antarctica. *Cryosphere*, 17: 3593–3616
- Pritchard H D, Arthern R J, Vaughan D G, Edwards L A. 2009. Extensive dynamic thinning on the margins of the Greenland and Antarctic ice sheets. *Nature*, 461: 971–975
- Pritchard H D, Ligtenberg S R M, Fricker H A, Vaughan D G, van den Broeke M R, Padman L. 2012. Antarctic ice-sheet loss driven by basal melting of ice shelves. *Nature*, 484: 502–505
- Peltier W R, Argus D F, Drummond R. 2018. Comment on “An Assessment of the ICE-6G_C (VM5a) Glacial Isostatic Adjustment Model” by Purcell et al. *J Geophys Res-Solid Earth*, 123: 2019–2028
- Qiu J. 2017. Antarctica’s sleeping ice giant could wake soon. *Nature*, 544: 152–154
- Ribeiro N, Herraiz-Borreguero L, Rintoul S R, McMahon C R, Hindell M, Harcourt R, Williams G. 2021. Warm modified circumpolar deep water intrusions drive ice shelf melt and inhibit dense shelf water formation in Vincennes Bay, East Antarctica. *J Geophys Res-Oceans*, 126: 17
- Rignot E, Mouginot J, Scheuchl B, van den Broeke M, van Wessem M J, Morlighem M. 2019. Four decades of Antarctic Ice Sheet mass balance from 1979–2017. *Proc Natl Acad Sci USA*, 116: 1095–1103
- Sasgen I, Martinec Z, Bamber J. 2010. Combined GRACE and InSAR estimate of West Antarctic ice mass loss. *J Geophys Res*, 115: 9
- Sasgen I, Martín-Español A, Horvath A, Klemann V, Petrie E J, Wouters B, Horwath M, Pail R, Bamber J L, Clarke P J, Konrad H, Wilson T, Drinkwater M R. 2018. Altimetry, gravimetry, GPS and viscoelastic modeling data for the joint inversion for glacial isostatic adjustment in Antarctica (ESA STSE Project REGINA). *Earth Syst Sci Data*, 10: 493–523
- Sasgen I, Wouters B, Gardner A S, King M D, Tedesco M, Landerer F W, Dahle C, Save H, Fettweis X. 2020. Return to rapid ice loss in Greenland and record loss in 2019 detected by the GRACE-FO satellites. *Commun Earth Environ*, 1: 8
- Schrama E J O, Wouters B, Rietbroek R. 2014. A mascon approach to assess ice sheet and glacier mass balances and their uncertainties from GRACE data. *J Geophys Res-Solid Earth*, 119: 6048–6066
- Schröder L, Horwath M, Dietrich R, Helm V, van den Broeke M R, Ligtenberg S R M. 2019. Four decades of Antarctic surface elevation changes from multi-mission satellite altimetry. *Cryosphere*, 13: 427–449
- Shen Q, Wang H, Shum C K, Jiang L, Hsu H T, Dong J. 2018. Recent high-resolution Antarctic ice velocity maps reveal increased mass loss in Wilkes Land, East Antarctica. *Sci Rep*, 8: 4477
- Shepherd A, Ivins E, Rignot E, Smith B, van den Broeke M, Velicogna I, Whitehouse P, Briggs K, Jouguin I, Krinner G, Nowicki S, Payne T, Scambos T, Schlegel N, Agosta C, Ahlström A, Babonis G, Barletta V, Blazquez A, Bonin J, Csatho B, Cullather R, Felikson D, Fettweis X, Forsberg R, Gallee H, Gardner A, Gilbert L, Groh A, Gunter B, Hanna E, Harig C, Helm V, Horvath A, Horwath M, Khan S, Kjeldsen K K, Konrad H, Langen P, Lecavalier B, Loomis B, Luthcke S, McMillan M, Melini D, Mernild S, Mohajerani Y, Moore P, Mouginot J, Moyano G, Muir A, Nagler T, Nield G, Nilsson J, Noel B, Otosaka I, Pattle M E, Richard Peltier W, Pie N, Rietbroek R, Rott H, Sandberg-Sørensen L, Sasgen I, Save H, Scheuchl B, Schrama E, Schröder L, Seo K-W, Simonsen S, Slater T, Spada G, Sutterley T, Talpe M, Tarasov L, van de Berg W J, van der Wal W, van Wessem M, Vishwakarma B D, Wiese D, Wouters B. 2018. Mass balance of the Antarctic Ice Sheet from 1992 to 2017. *Nature*, 558: 219
- Shepherd A, Gilbert L, Muir A S, Konrad H, McMillan M, Slater T, Briggs K H, Sundal A V, Hogg A E, Engdahl M E. 2019. Trends in Antarctic Ice Sheet elevation and mass. *Geophys Res Lett*, 46: 8174–8183
- Silva A B, Arigony-Neto J, Braun M H, Espinoza J M A, Costi J, Jaña R. 2020. Spatial and temporal analysis of changes in the glaciers of the Antarctic Peninsula. *Glob Planet Change*, 184: 103079
- Smith B, Fricker H A, Gardner A S, Medley B, Nilsson J, Paolo F S, Holschuh N, Adusumilli S, Brunt K, Csatho B, Harbeck K, Markus T, Neumann T, Siegfried M R, Zwally H J. 2020. Pervasive ice sheet mass loss reflects competing ocean and atmosphere processes. *Science*, 368: 1239–1242
- Stokes C R, Abram N J, Bentley M J, Edwards T L, England M H, Foppert A, Jamieson S S R, Jones R S, King M A, Lenaerts J T M, Medley B, Miles B W J, Paxman G J G, Ritz C, van de Flierdt T, Whitehouse P L. 2022. Response of the East Antarctic Ice Sheet to past and future climate change. *Nature*, 608: 275–286
- Su X, Shum C K, Guo J, Howat I M, Kuo C, Jezek K C, Duan J, Yi Y. 2018. High-resolution interannual mass anomalies of the Antarctic Ice Sheet by combining GRACE gravimetry and ENVISAT altimetry. *IEEE Trans Geosci Remote Sens*, 56: 539–546
- Sun Y, Riva R, Ditmar P. 2016. Optimizing estimates of annual variations and trends in geocenter motion and J_2 from a combination of GRACE data and geophysical models. *J Geophys Res-Solid Earth*, 121: 8352–8370
- Tapley B D, Watkins M M, Flechtner F, Reigber C, Bettadpur S, Rodell M, Sasgen I, Famiglietti J S, Landerer F W, Chambers D P, Reager J T, Gardner A S, Save H, Ivins E R, Swenson S C, Boening C, Dahle C, Wiese D N, Dobslaw H, Tamisiea M E, Velicogna I. 2019. Contributions of GRACE to understanding climate change. *Nat Clim Chang*, 9: 358–369
- Tikhonov A N. 1963a. Regularization of ill-posed problems. *Dokl Akad Nauk SSSR*, 151: 49–52
- Tikhonov A N. 1963b. Solution of incorrectly formulated problems and the regularization method. *Dokl Akad Nauk SSSR*, 151: 501–504
- Undén P, Rontu L, Jarvinen H, Lynch P, Calvo J, Cats G, Cuxart J, Eerola K, Fortelius C, Garcia-moya J, Jones C, Lenderlink G, McDonald A, McGrath R, Navascues B. 2002. *HIRLAM-5 Scientific Documentation. Technical Report*. Swedish Meteorology and Hydrology Institute
- van Wessem J M. 2016. High resolution climate modelling of Antarctica and the Antarctic Peninsula. Dissertation for Doctoral Degree. Utrecht: Utrecht University
- van Wessem J M, van de Berg W J, Noël B P Y, van Meijgaard E, Amory C, Birnbaum G, Jakobs C L, Krüger K, Lenaerts J T M, Lhermitte S, Ligtenberg S R M, Medley B, Reijmer C H, van Tricht K, Trusel L D, van Ulft L H, Wouters B, Wuite J, van den Broeke M R. 2018. Modelling the climate and surface mass balance of polar ice sheets using RACMO2—Part 2: Antarctica (1979–2016). *Cryosphere*, 12: 1479–1498
- Veldhuijsen S B M, van de Berg W J, Brils M, Kuipers Munneke P, van den Broeke M R. 2023. Characteristics of the 1979–2020 Antarctic firm layer simulated with IMAU-FDM v1.2A. *Cryosphere*, 17: 1675–1696
- Velicogna I, Sutterley T C, van den Broeke M R. 2014. Regional acceleration in ice mass loss from Greenland and Antarctica using GRACE time-variable gravity data. *Geophys Res Lett*, 41: 8130–8137
- Velicogna I, Mohajerani Y, Geruo A, Landerer F, Mouginot J, Noel B, Rignot E, Sutterley T, van den Broeke M, van Wessem M, Wiese D. 2020. Continuity of Ice Sheet mass loss in Greenland and Antarctica from the GRACE and GRACE Follow-On missions. *Geophys Res Lett*,

- 47: 8
- Wang W, Shen Y Z, Chen Q J, Wang F W. 2023a. Unprecedented mass gain over the Antarctic ice sheet between 2021 and 2022 caused by large precipitation anomalies. *Environ Res Lett*, 18: 124012
- Wang W, Shen Y Z, Chen Q J, Chen T Y. 2023b. One-degree resolution mascon solution over Antarctic derived from GRACE Level-2 data. *Front Earth Sci*, 11: 1129628
- Wang W, Shen Y Z, Chen Q J, Wang F W. 2024. A data-driven method for enhancing spatial resolution in estimating terrestrial water storage changes from satellite gravimetry. *IEEE Geosci Remote Sens Lett*, 21: 1503105
- Whitehouse P L, Bentley M J, Milne G A, King M A, Thomas I D. 2012. A new glacial isostatic adjustment model for Antarctica: Calibrated and tested using observations of relative sea-level change and present-day uplift rates. *Geophys J Int*, 190: 1464–1482
- Willen M O, Horwath M, Buchta E, Scheinert M, Helm V, Uebbing B, Kusche J. 2024. Globally consistent estimates of high-resolution Antarctic ice mass balance and spatially resolved glacial isostatic adjustment. *Cryosphere*, 18: 775–790
- Witze A. 2018. East Antarctica is losing ice faster than anyone thought. *Nature*, <http://doi.org/10.1038/d41586-018-07714-1>
- Yang T, Liang Q, Zheng L, Li T, Chen Z, Hui F, Cheng X. 2023. Mass balance of the Antarctic Ice Sheet in the early 21st century. *Remote Sens*, 15: 1677
- Yu Y, Yang L, Shen Y, Wang W, Li B, Chen Q. 2024. An iterative and shrinking generalized ridge regression for ill-conditioned geodetic observation equations. *J Geod*, 98: 3
- Yue L, Chao N, Chen G, Chen L, Zhang B, Sun R, Zhang Y, Wang S, Wang Z, Li F, Yu N, Ouyang G. 2023. Reconstructing continuous ice sheet elevation changes in the Amundsen sea sector during 2003–2021 by merging Envisat, ICESat, CryoSat-2, and ICESat-2 multi-altimeter observations. *J Geophys Res-Earth Surf*, 128: e2022JF007020

(Editorial handling: Jiancheng SHI)